FAZ Publishing
JCF

Journal of Complex Flow, Vol. 3 No. 1 (2021) p. 26-31

Journal of Complex Flow

Journal homepage : www.fazpublishing.com/jcf

e-ISSN : 2672-7374

Numerical Study of Jet Impingement Cooling on Smooth Concave Surfaces

Ummi Nazihah Nuruddin[1,a], Suzairin Md Seri[2,b]

[1]Faculty of Mechanical and Manufacturing Engineering,
Universiti Tun Hussein Onn Malaysia, Batu Pahat, 86400, MALAYSIA

[2] Centre for Energy and Industrial Environment Studies (CEIES),
Faculty of Mechanical and Manufacturing Engineering, Universiti Tun Hussein Onn Malaysia, 86400 Parit Raja, Batu Pahat, Johor Darul Takzim, MALAYSIA

*Corresponding Author

Email: suzairin@uthm.edu.my

Received 12 November 2020;
Accepted 4 January 2021;
Available online 30 April 2021

Abstract: Jet impingement cooling is one of the best methods to improvise the coefficient of heat transfer. Since there are few studies of impingement on concave surfaces, a numerical study of jet impingement cooling is needed to investigate the effect of the nozzle tip to the impingement surface distance and the radius of curvature of the impingement surface at various Reynolds numbers on the thermal performance of the jet impingement cooling. The main objective of this study is to produce a mathematical correlation that relates all of the parameters considered to the thermal performance of the present jet impingement cooling system. It is found that Reynold numbers and geometry of the system influence the rate of heat transfer. Computational Fluid Dynamics is the method used in this study and the simulation is run using ANSYS Fluent. Out of all turbulence models examined, the best-validated result was achieved with the K-epsilon RNG model applied to the simulations. The correlation was tested by comparing the outcome of the correlation with the results of the simulations. The normalized root means square error, NRMSE, obtained indicates that the ACFD correlation is acceptable and applicable to be used for future reference

Keywords: Jet impingement cooling, Concave surface, Heat transfer coefficient

1. Introduction

Jet impingement cooling is one of the best methods to remove large amount of heat from solid surfaces. The coefficient of heat transfer in jet impingement is almost twice than conventional method. It is widely used in many applications such as gas turbines, paper drying, high-density electronic equipment as it has high local convective heat transfer rate, inexpensive and effective [1]. Many studies are involving mainly flat surfaces and little data is available for non-flat surface geometries or curve impingement surfaces such as concave surface [2]. Surface curvature increases the average Nusselt number which increase the cooling performance [3].

Impingement happens when there is a collision between the coolant flow and the target surface. Jet impingement flow from a very thin boundary layer hence resulting in an extremely large heat transfer coefficient. Impingement heat transfer also affected by turbulence levels at the nozzle exit, which depend on its diameter and length [4]. The Reynold number plays a major role in the heat transfer performance [5]. To determine a heat transfer through jet impingement is quite complex and depends on many factors such as Reynold numbers, Prandtl number, Nusselt number, jet diameter and wall-to-nozzle spacing.

The objective of this study is to investigate the characteristic of thermal and flow field on curve surfaces caused by jet impingement. Other than that, this study is significant to obtain correlations that relates the flow geometries and Reynold numbers towards the thermal and overall performance of jet impingement cooling systems. For the simulations work, scopes, nozzle tip to impingement surface distance is ranging from 1 to 6 times the nozzle width. The concave surface radius of curvature is ranging from 4 to 15 times the nozzle width. Reynold numbers set between 5000 to 100000.

**Corresponding author: suzairin@uthm.edu.my*

2. Modelling and Methodology

A 2-D axis-symmetry round nozzle with a convex target surface was drawn in the SolidWorks and later it was imported to the ANSYS Fluent R3 Student Version. The dimensions and related parameters were obtained from the previous experiment that was investigated by Lee *et al*. [6]. The validation between experimental result and simulation was done after performing a grid independence test.

2.1 Governing equations

Based on the scope of this study, the geometry was in a 2-D but axis-symmetry geometry. Hence, the directions of the velocities were classified into two directions which are *x* and *y* direction. The fluid flow was set to be incompressible and steady flow. So, the continuity equation is given by,

$$\frac{\partial u}{\partial x}+\frac{\partial v}{\partial y}=0 \tag{1}$$

The momentum equations in *x* and *y* direction are given as the following equations respectively.

$$\rho u\frac{\partial u}{\partial x}+\rho v\frac{\partial u}{\partial y}=-\frac{\partial \hat{p}}{\partial x}+\mu\left(\frac{\partial^2 u}{\partial x^2}+\frac{\partial^2 u}{\partial y^2}\right) \tag{2}$$

$$\rho u\frac{\partial v}{\partial x}+\rho v\frac{\partial v}{\partial y}=-\frac{\partial \hat{p}}{\partial y}+\mu\left(\frac{\partial^2 v}{\partial x^2}+\frac{\partial^2 v}{\partial y^2}\right) \tag{3}$$

The parameters were selected by referring to parameters of jet impingement model on experimental data of Lee et al. [6] added with another geometrical parameter. Table 1 shows the dimension of fluid domain. Reynold number is set as manipulated variable in this journal, hence value of Reynold number from range of 5000 to 100000 is chosen. Table 1 shows the parameters, properties and the dimension of fluid domain which used to do the geometry modelling.

Table 1 – Parameters selection

Impinged surface shape	Concave
Type of fluid	Air
S, The target surface periphery (mm)	598.5
L, nozzle-to-surface distance / mm	21.5, 43, 86, 129
d, nozzle diameter / mm	21.5
Z, nozzle distance / mm	Z = 58d
Re, Reynold number	5000 - 100000

The geometry of the structure of jet impingement is modelled based on the parameter selection. The computational domain is sketched in ANSYS Workbench of Design Modeler. Fig. 1(a) shows the computational domain for nozzle distance, nozzle-to-distance surface, and radius of inner diameter of concave surface while Fig. 1(b) shows the computational domain for nozzle width. As for Fig. 1(c), it shows the close-up view for curve length of concave surface, *S* = 59.85 cm.

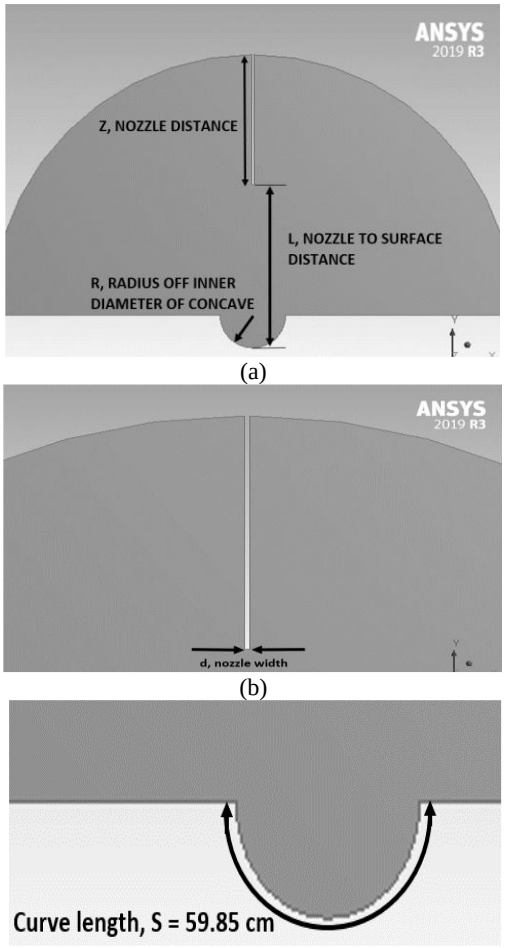

Fig. 1 – (a) The geometry of fluid domain drawn in Design Modeler (b) The closed-up geometry of nozzle (c) Curve length of concave surface

2.2 Boundary conditions

The first step in setting up the boundary condition, by giving names according to its design region such as inlet, outlet, and wall. Inlet boundary is where the air enters the nozzle. The inlet boundary is where the velocity is set. The inlet velocity, *Vin* is calculated with respective of the Reynolds numbers, *Re*, and the width of the nozzle, d. Atmospheric pressure is set at the outlet region. No-slipped condition is applied to all the walls. Fig. 2 shows the computational domain. Table 2 shows the boundary operating conditions.

Table 2 – Boundary operating conditions

Inlet	Type of boundary	Velocity-inlet
	V_{in} (m/s)	$V_{in}=Re(\mu)/\rho d$
Outlet	Type of boundary	Pressure-outlet
	Pressure (Pa)	0 gauges pressure
Wall	Shear condition	No-slip
Working fluid properties	Working fluid	Air
	Temperature (K)	300
	Density, ρair (kg/m3)	1.225
	Viscosity, (kg/m.s)	1.7894x10-5

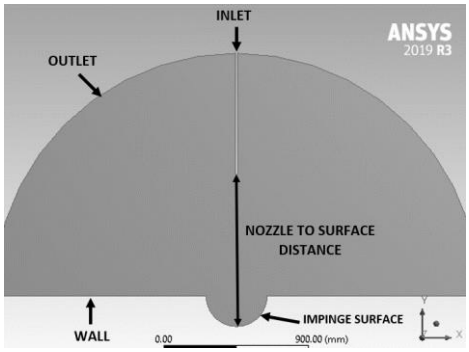

Fig. 2 – Setup boundary condition region

2.3 Grid independence test

For the grid independence study, the simulation is run using the variable of *R/d*=5.6, *L/d*=2 and *Re*=23000. This test is significant to ensure that the truncation error and the round-off error from the meshing do not give impact to the simulation results and to ensure that simulation results are independent of the size of the meshing cells. Table 3 shows the number of nodes from each meshing by using different meshing density. Fig. 3 shows the comparison graph of surface Nusselt number against curve length for different modifications.

Table 2 – Boundary operating conditions

No of nodes	Average Nusselt number
24132	70.518
18921	70.252
14328	70.171
13045	71.742
12038	70.172

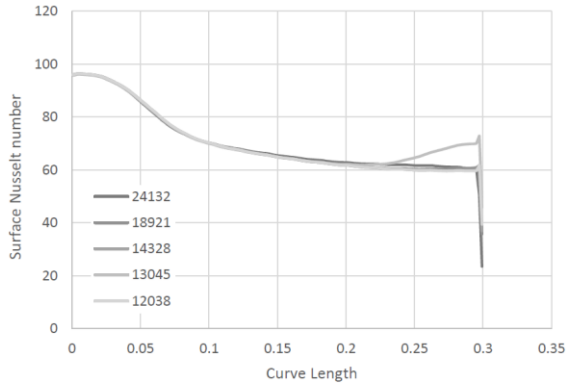

Fig. 3 – Surface Nusselt number vs curve length

According to the grid independence test result shown in figure 3, the numerical results of local Nusselt number distribution remain unchanged for most gird density except for one, which has meshing of 24132 nodes. Any mesh density that produces similar results is useable since the present work is in 2-dimensional and an increment in mesh density does not give major effect on the computational time. The meshing with a cell growth rate of 1.05 is chosen for validation work and predictive simulations.

3. Validations

A qualitative and quantitative comparison between the average Nusselt number from the simulations with experimental data was made. The results of the average Nusselt number of the concave surface for *L/d*=2 and *R/d*=5.6 were used for comparison. Fig. 4 shows the qualitative comparison between data. Meanwhile, the quantitative comparison was made by using normalized root mean square error, NRMSE, and the result is shown in Table 3. It seems that the turbulence model of K-epsilon RNG gives the smallest value of NRMSE which is 0.03897. Hence, the turbulence model of *K*-epsilon RNG was used on other simulations for predictive results.

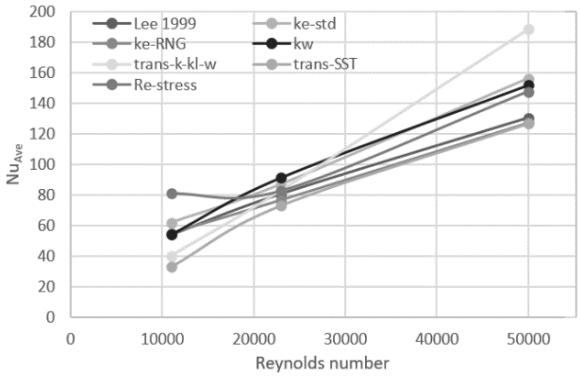

Fig. 4 – Comparison graph for Nu_{ave} against *Re* for each turbulent model

Table 3 – NRMSE result for each turbulent model

Turbulent Model	NRSME
K-epsilon standard	0.21024
K-epsilon RNG	0.03897
K-omega	0.81257
Transition k-kl-omega	0.45454
Transition-SST	0.71356
Reynold stress	0.24302

4. Results and Discussions

4.1 Correlation of different parameters

Graph of Nu_{ave} against Re shown in Fig. 5 shows a linear line and the value of Reynold numbers increases, the average Nusselt number increases too. As for Nu_{Ave} against *L/d* shown in Fig. 6, it can be observed that the value of average Nusselt number decreases when L/d increases from 1 to 2. Beyond this point, the Nu_{ave} is practically a constant value. Meanwhile for Nu_{ave} against *R/d* shown in Fig. 7, there are no major differences occur in changing of average Nusselt number for each radius curvature of concave surfaces.

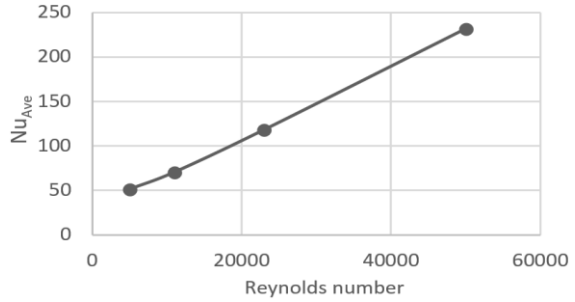

Fig. 5 - Nusselt number vs Reynold number

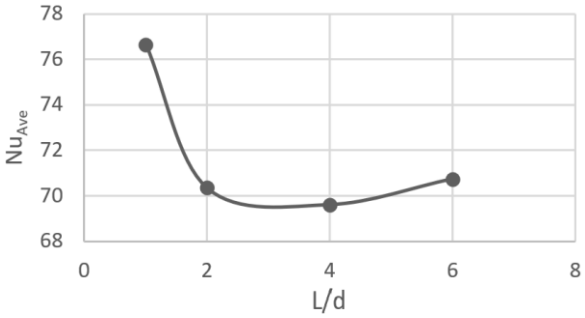

Fig. 6 – Nusselt number vs *L/d*

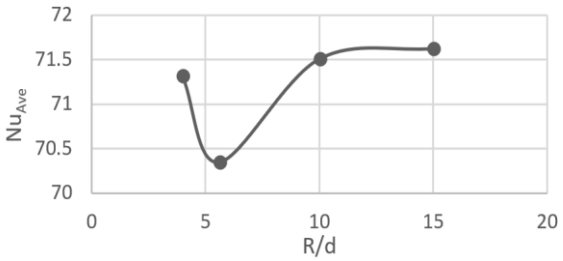

Fig. 7 – Nusselt number vs *R/d*

4.2 Asymptotic Computational Fluid Dynamics

Asymptotic Computational Fluid Dynamics, (ACFD), was used to produce a correlation between all the relevant non-dimensional variables analyzed by CFD. The relationship between the dependent variable of average Nusselt number and each of the independent variables (*Re*, *L/d* and *R/d*) was linearized by modifying the independent variables, which are known as phis, ∅i. *Phi*, ∅, is used as the new *x*-axis replacing the initial x-axis from the graph of Nu_{Ave} vs *Re*, Nu_{Ave} vs *L/d* and Nu_{Ave} vs *R/d* becoming Nu_{Ave} vs $Ø_1$, Nu_{Ave} vs $Ø_2$, and Nu_{Ave} vs $Ø_3$, respectively. The values for each phi, ∅ are based from the curved-fit equation obtained from graph as shown in figure 8-10. The *x* in the equation is substituted with corresponding parameters of *Re*, *L/d* and *R/d* as shown in Table 4-6. A linearization graph of Nu_{Ave} vs *Ø* is plotted using the tabulated data and the linearized graph is shown in Fig. 11-13. After linearization is done for each phi, *Ø*, combinations of all phis, $Ø_i$ are plotted in one graph as shown in Fig. 14.

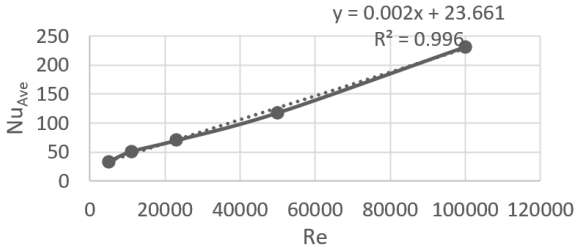

$$Ø_1 = 0.002x + 23.661$$

Fig. 8 –Correlation for Nusselt number and Re with the equation

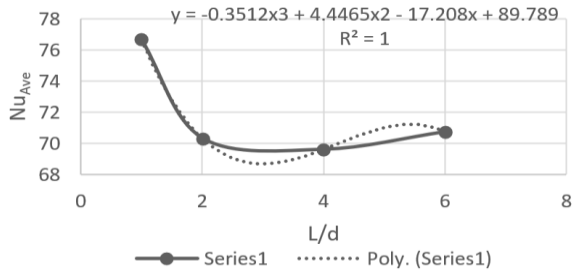

$$Ø_2 = -0.3512\,x^3 + 4.4465\,x^2 - 17.208x + 89.789$$

Fig. 9 – Correlation for Nusselt number and L/d with the equation

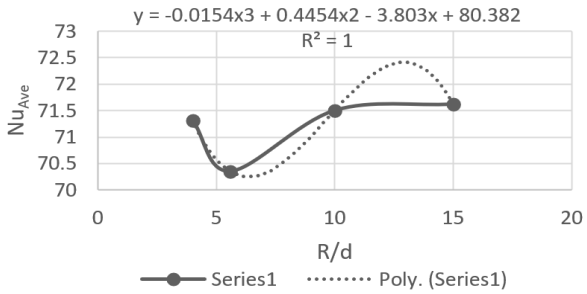

$$Ø_3 = -0.0154\,x^3 + 0.4454\,x^2 - 3.803x + 80.382$$

Fig. 10 – Correlation for Nusselt number and R/d with the equation

Table 4 – The value of Re, $Ø_1$, and Nu_{ave}

Re	$Ø_1$	Average Nusselt number (Nu_{ave})
5000	33.661	33.6307
11000	45.661	51.2109
23000	69.661	70.3503
50000	123.661	118.0068
100000	223.661	231.7377

Table 5 – The value of L/d, $Ø_2$, and Nu_{ave}

L/d	$Ø_2$	Average Nusselt number (Nu_{ave})
1	76.6763	76.6767
2	70.3494	70.3503
4	69.6242	69.6264
6	70.7558	70.7597

Table 6 – The value of R/d, $\emptyset_3$ and Nu_{ave}

R/d	$\emptyset_1$	Average Nusselt number (Nu_{ave})
4	71.3108	71.3114
5.6	70.3485	70.3503
10	71.4920	71.5044
15	71.5770	71.6218

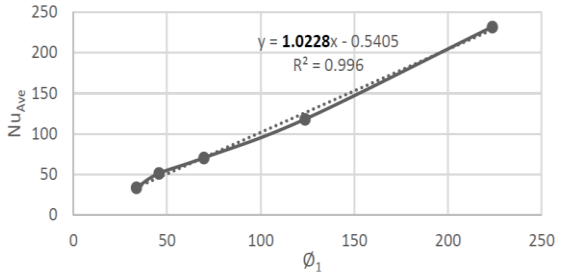

Fig. 11 – Linearization graph of average Nusselt number, $Nuave$ against $\emptyset 1$

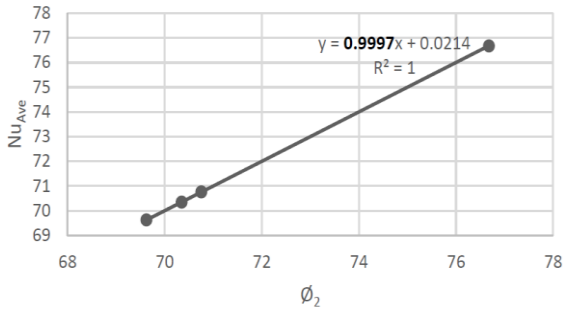

Fig. 12 – Linearization graph of average Nusselt number, $Nuave$ against $\emptyset 2$

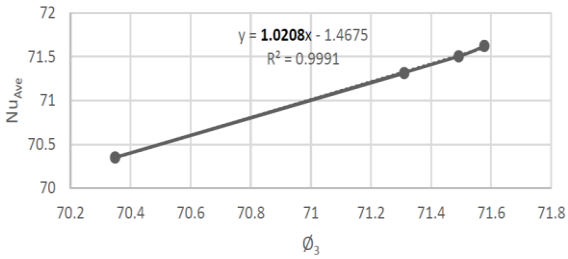

Fig. 13 – Linearization graph of average Nusselt number, $Nuave$ against $\emptyset 3$

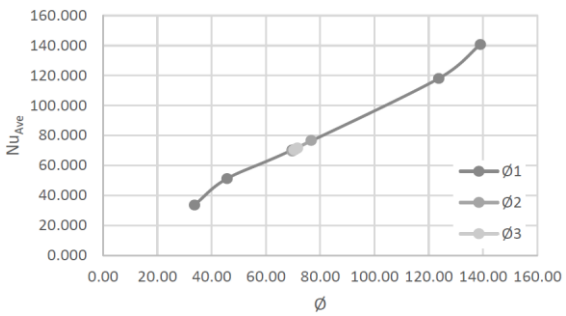

Fig. 14 – Combination of all phi, Ø

From the graph, all linear lines for each phi, $\emptyset$ intersect with each other. However, the line for series 1 which represent $\emptyset_1$ is longer than the $\emptyset_2$ and $\emptyset_3$. This is due to $\emptyset_1$ has a greater effect of average Nusselt number compare to the others. In this combination, there is one value of average Nusselt number that is common for all $\emptyset$, which is Nu_{ave} = 70.350. This value is the $Nu_{Ave,ref}$ in the Taylor series expansion. The gradient is based on the curve-fit equation obtained from the graph is substitute into $\delta Nu_{ave}/\delta\emptyset$. The new value of $\emptyset_{ref}$ is calculated using derivation from equation (4). The result is tabulated in table 7.

$$Nu_{Ave} = Nu_{Ave,ref} + (\emptyset_1 - \emptyset_{1ref})(\delta Nu_{Ave} / \delta\emptyset_1) + (\emptyset_2 - \emptyset_{2ref})(\delta Nu_{Ave} / \delta\emptyset_2) + (\emptyset_3 - \emptyset_{3ref})(\delta Nu_{Ave} / \delta\emptyset_3) \quad (4)$$

Table 7 – Taylor series expansion variables with Nu_{ave} = 70.350 as the reference value

Parameter		$\emptyset_{ref}$		$\delta Nu_{Ave}/\delta\emptyset$
Re	23000	$\emptyset_{1ref}$	69.66	1.0288
L/d	2	$\emptyset_{2ref}$	70.35	0.9997`
R/d	5.6	$\emptyset_{3ref}$	70.35	1.0208

The average Nusselt numbers obtained from simulations, $Nu_{ave,sim}$, were compared to the average Nusselt number obtained from ACFD, $Nuave,ACFD$ and the comparison is shown in figure 15 and table 8.

Table 8 - Comparison average Nusselt number for simulation and ACFD

Re	L/d	R/d	Nu_{Ave}	
			Simulation	ACFD
5000	2	5.6	33.6307	33.3121
11000	2	5.6	51.2109	45.6577
23000	2	5.6	70.3503	70.3489
50000	2	5.6	118.007	125.904
100000	2	5.6	231.738	228.784
23000	1	5.6	76.6767	76.6739
23000	4	5.6	69.6264	69.6239
23000	6	5.6	70.7597	70.7551
23000	2	10	71.5044	71.5162
23000	2	15	71.6218	71.603

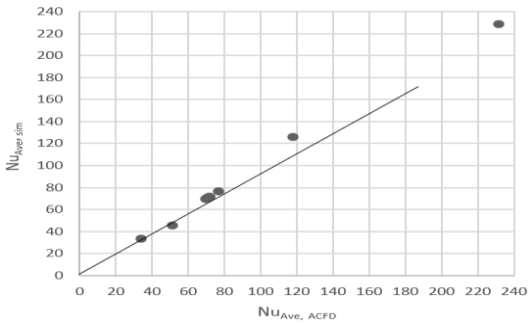

Fig. 15 – Parity plot of average Nusselt number between simulations and ACFD

According to Fig. 15 and Table 8, the ACFD correlation is in good agreement with the numerical results. The normalized root means square error, NRMSE, is found to be 0.01537 or 1.537%.

5. Conclusion

The parameters such as Reynolds number, nozzle-tip-to-impingement-surface distance, and radius of curvature of the concave surface influence the convective heat transfer rate. The Nusselt number increases when there is an increase in the Reynolds number. As for nozzle-tip-to-impingement-surface distance (*L/d*), the Nusselt number decreases from *L/d* equals to 1 to *L/d* equals to 2. The Nusselt number barely changes when the *L/d* further increases. In the matter of radius curvature of the concave surface, the Nusselt number is found to slightly change when the radius of surface curvature changes. A correlation, that represents Nu_{Ave} as a function of *Re*, *L/d*, and *R/d*, was produced through ACFD method. The comparison between the average Nusselt number of the simulations and ACFD was made and the NRMSE is found to be 0.01537 or 1.537%. This value indicates that the correlation of ACFD is acceptable and applicable to be used for this study or future reference.

Acknowledgement

The authors thank to the all industries partner and Universiti Tun Hussein Onn Malaysia (UTHM) for the award of grant and equipment support for the project.

Reference

[1] E. Baydar and Y. Ozmen, "An experimental and numerical investigation on a confined impinging air jet at high Reynolds numbers," *Appl. Therm. Eng.*, vol. 25, no. 2–3, pp. 409–421, 2005.

[2] G. Yang, M. Choi, and J. S. Lee, "An experimental study of slot jet impingement cooling on concave surface: Effects of nozzle configuration and curvature," *Int. J. Heat Mass Transf.*, vol. 42, no. 12, pp. 2199–2209, 1999.

[3] E. Öztekin, O. Aydin, and M. Avci, "Heat transfer in a turbulent slot jet flow impinging on concave surfaces," *Int. Commun. Heat Mass Transf.*, vol. 44, pp. 77–82, 2013.

[4] S. V. Garimella and B. Nenaydykh, "Nozzle-geometry effects in liquid jet impingement heat transfer," *Int. J. Heat Mass Transf.*, vol. 39, no. 14, pp. 2915–2923, 1996.

[5] T. L. Chan, C. W. Leung, K. Jambunathan, S. Ashforth-Frost, Y. Zhou, and M. H. Liu, "Heat transfer characteristics of a slot jet impinging on a semi-circular convex surface," *Int. J. Heat Mass Transf.*, vol. 45, no. 5, pp. 993–1006, 2002.

[6] D. H. Lee, Y. S. Chung, and S. Won, "The effect of concave surface curvature on heat transfer from a fully developed round impinging jet," pp. 1378–1386, 1999.